Eur. Phys. J. Plus (2021) 136:457
https://doi.org/10.1140/epjp/s13360-021-01461-5

THE EUROPEAN PHYSICAL JOURNAL PLUS

Regular Article

Swapping of orbital angular momentum states of light in a quantum well waveguide

Seyyed Hossein Asadpour[1], Edris Faizabadi[1], Viaceslav Kudriašov[2], Emmanuel Paspalakis[3], Hamid. R. Hamedi[2,a]

[1] School of Physics, Iran University of Science and Technology, 1684613114 Tehran, Iran
[2] Institute of Theoretical Physics and Astronomy, Vilnius University, Saulėtekio 3, Vilnius 10257, Lithuania
[3] Materials Science Department, School of Natural Sciences, University of Patras, Patras 265 04, Greece

Received: 15 February 2021 / Accepted: 19 April 2021

Abstract We study the effect of orbital angular momentum transfer between optical fields in a semiconductor quantum well waveguide with four energy levels in a closed-loop configuration via four-wave mixing. The waveguide is driven by two strong control fields and two weak probe fields. We consider three different cases for the light-matter interaction in order to efficiently exchange optical vortices. In the first two cases, the system is initially prepared in either a lower electromagnetically induced transparency or a coherent population trapping state, while the last case prepares the system in an upper state, enabling to induce the electron spin coherence. We find that for appropriate parameters and via the spin coherence effect, the efficiency of four-wave mixing is much higher in the quantum well waveguide. Working in the electron spin coherence regime, we then study the light-matter interaction under the situation where only one of the control fields has an optical vortex. The orbital angular momentum of the vortex control beam can be efficiently transferred to a generated probe field via the spin coherence. We also show that the spatially dependent optical effects of the waveguide can be strongly modified by the electron spin coherence.

1 Introduction

The coherent interaction of light with atoms is responsible for many essential phenomena, and enables to study new research directions. Various combinations of atomic interactions and electromagnetic fields has disclosed important optical effects such as electromagnetically induced transparency (EIT) [1,2], stimulated Raman adiabatic passage (STIRAP) [3,4], refractive index enhancement or change into negative sign [5,6], manifestation of slow, stored, or fast light [7–11], lasing without inversion [12], giant Kerr nonlinearity [13–16], and more. All of the phenomena are realized experimentally and have a potential for the practical application. The slow and stored light can be explored in reversible quantum memories [17–20] or in rotation sensors [21,22], optical switchers [23], and atomic clocks [24].

Similar quantum-coherence phenomena as in cold atomic media have been in parallel studying in semiconductors, which, in particular in quantum structures (like quantum dots

[a] e-mail: hamid.hamedi@tfai.vu.lt (corresponding author)

or wells) exhibit an ability to tune a band gap by modification of the structure's geometry. Thus, these structures with tunable properties acting as artificial atoms extend the potential for their application in optoelectronics and quantum information science [25–30].

The preparation of media into coherent superposition of ground or metastable state (so-called dark state) results in an effect, known as coherent population trapping (CPT). In its simplest case, the state can be the result of quantum interference in a three-level Λ system. The same system is used to explore EIT, which requires two-photon resonance condition. More available three-level systems like V-type or cascade-type have been investigated and compared [31–33]; however, only Λ system exhibits complete transparency.

Light beams can carry an orbital angular momentum (OAM) [34,35]. This feature provides additional possibilities for the manipulation of light as it represents another degree of freedom, which is suitable for the application in the quantum computation, quantum teleportation, and quantum information storage [35–40]. In the Λ system, the scenario of slow, stored and restored light in many previous works have been accomplished by using strong so-called control beam and much weaker incident probe beam which can carry an OAM [41–44]. Another scenario can be implemented with the control beam carrying the OAM. However, the intensity of the beam with OAM has an optical vortex profile, and at the center of the beam, the intensity goes to zero, resulting into the absorption losses of the probe beam. The solution to adiabatically suppress these losses is obtained by modifying the three-level system by coupling it to more light beams of strong intensity. This may be achieved, for example, by converting the Λ system to tripod [45,46] or double-Λ [24,47–50] schemes.

In semiconductors, EIT has been demonstrated by using nonradiative quantum coherences [30], via electron spin coherence (ESC) in a quantum well waveguide [27,51,52] or by intersubband transitions [53]. The intersubband optical transitions in semiconductors enable to exploit the quantum coherence for the observation of the different quantum phenomena, including gain without inversion, coherent control of absorption and dispersion, and four-wave mixing (FWM) [54–63]. The spin-related coherences are equally attractive and additionally have longer lifetimes than intersubband transitions. The spin coherence is related to the conservation of the total spin, and in the absence of magnetic field, the flip of the spin may be realized with the polarized light. In $AlGaAs/GaAs$ quantum wells, two upper doubly degenerate states are formed from electron spin states in a conduction band and the lower two states are the doubly degenerate light hole states in a valence band [27,64].

Recently, attention has been given to the interaction of intersubband quantum well transitions with light fields carrying OAM [65–67]. This work is focused on a four energy-level medium interacting with four light beams forming a closed-loop configuration similar to the schemes described in [51,52]. Because of the symmetry obtained in geometrical representation of the levels and the beams, the same system may be treated as double Λ or double-V structures. The distinction of the sub-systems may be considered in one case by attributing the intensities of the beams either as two strong beams for one strong sub-system and two weak beams for the weak sub-system, or another case as one strong and one weak beam for one subsystem and the rest of the beams for the another sub-subsystem. In the following, the system, in general, is characterized by five kinetic equations, and then further assumptions are used to obtain analytical relations. Three different cases are studied and compared. In the first two situations, the system is initially populated in a lower EIT-state or CPT-superposition state. In the third case, the system is prepared initially in an upper state which enables to induce the electron spin coherence (ESC). It is found that for proper parameters, the ESC results in a high-efficiency FWM in the quantum well waveguide. Assuming a situation where only one of the control fields has an optical vortex and taking into account the effect of ESC, the optical vortex of control beam can be transferred to a generated probe field with a high efficiency.

It is also shown that the position-dependent optical effects of the waveguide system can be well-controlled by the ESC. The dipole interaction, rotating wave approximation and density matrix formalism are used to calculate the energy-level population evolution, and slowly varying envelope approximation is exploited for the description of the electromagnetic field evolution.

2 Formulation

Let us consider a double Λ-type (or double-V) quantum well (QW) waveguide system. The valence-band states are labeled with J_z and the conduction-band states are labeled with $S_z = 1/2$ (spin up) and $S_z = -1/2$ (spin down). The polarization selection rule for the dipole transitions rules between the conduction band and the light hole (LH) valence band in the QW waveguide in the absence of an external magnetic field, where the two electron spin states can couple to a common LH valence-band state. Here, we consider three types of configuration in quantum well waveguide structure. In the first configuration (Fig. 1a), the sample interacts with a linear polarized weak probe field with Rabi frequency Ω_1 and a generating σ^+ polarized mixing field with Rabi frequency Ω_+. Moreover, the σ^- polarized field with Rabi frequency Ω_- and the linear polarized field with Rabi frequency Ω_2 as two strong coupling lights interact with the sample, respectively. While, in second one (Fig. 1b), the sample interacts with the linear polarized weak probe field with Rabi frequency Ω_1 and the σ^- generating polarized mixing field with Rabi frequency Ω_-. Moreover, the σ^+ polarized field with Rabi frequency Ω_+ and the linear polarized field with the Rabi frequency Ω_2 as two strong coupling lights interact with sample, respectively.

For the third assumption (Fig. 1c), we suppose that the condition for the presence of spin coherence is adapted. In this case, a strong field Ω_2 drives the transition from $|c\rangle$ to $|d\rangle$ and a weak probe field with Rabi frequency Ω_-, which is σ^-polarized, couples the transition $|c\rangle$ to $|a\rangle$. The electron spin coherence (ESC) can also be induced through the transition $|b\rangle$ to $|a\rangle$, which is driven by the mixing field, and the transition from $|b\rangle$ to $|d\rangle$ which is driven by the second strong σ^+ polarized field. Consequently, a coupled double-V scheme is formed.

The system under consideration may be viewed as consisting of two Λ or double-V subsystems coupled via four optical fields driving dipole-allowed transitions in a closed-loop configuration. Such a closed-loop system allows one of the fields to be generated out of the QW waveguide ensemble through the FWM process. In our study, we will be interested in three scenarios where the light-matter interaction is dominated either by EIT, CPT or via ESC. Specifically, we will be studying the effect of OAM (vortex) transfer between the fields propagating in this closed-loop system.

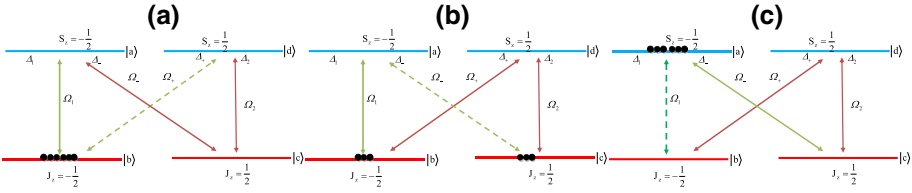

Fig. 1 Schematic of energy levels for the EIT (**a**), CPT (**b**) and ESC (**c**) cases

Taking the dipole and rotating wave approximation, in the interaction picture, the Hamiltonian can be written as

$$\begin{aligned} H_{int}^{I}/\hbar = {} & \Delta_1 \left|b\right\rangle \left\langle b\right| + \Delta_- \left|c\right\rangle \left\langle c\right| + (\Delta_- - \Delta_2) \left|d\right\rangle \left\langle d\right| \\ & - (\Omega_- \left|a\right\rangle \left\langle c\right| + \Omega_+ \left|d\right\rangle \left\langle b\right| + H.c.) \\ & - (\Omega_1 \left|a\right\rangle \left\langle b\right| + \Omega_2 \left|d\right\rangle \left\langle c\right| + H.c.) \end{aligned} \tag{1}$$

where the detunings are defined as $\Delta_1 = \omega_1 - \omega_{ab}$, $\Delta_- = \omega_- - \omega_{ac}$ and $\Delta_2 = \omega_2 - \omega_{dc}$. Here $\omega_{mn} = (\varepsilon_m - \varepsilon_n)/\hbar$ is the optical transition frequency $(m, n = a, b, c, d; m \neq n)$, $\varepsilon_{m(n)}$ is the energy of state $m(n)$, $\omega_j (j = 1, 2, \pm)$ shows the frequency of the corresponding laser; $\Omega_+ = (\boldsymbol{\mu}_{bd} \cdot \mathbf{e}_+)E_+/\hbar$, $\Omega_- = (\boldsymbol{\mu}_{ac} \cdot \mathbf{e}_-)E_-/\hbar$, $\Omega_1 = (\boldsymbol{\mu}_{ab} \cdot \mathbf{e}_1)E_1/\hbar$ and $\Omega_2 = (\boldsymbol{\mu}_{dc} \cdot \mathbf{e}_2)E_2/\hbar$ denote the corresponding Rabi frequencies with $\boldsymbol{\mu}_{mn}$ being the dipole moment for the relevant transition $|m\rangle \leftrightarrow |n\rangle$, and $E_j (j = \pm, 1, 2)$ and $\mathbf{e}_j$ being the corresponding electric field amplitude and the unit polarization vector of the electric field, respectively. We can write the density matrix elements as follows:

$$\begin{aligned} \dot{\rho}_{ab} = {} & i\left(\Delta_1 + i\gamma_1\right)\rho_{ab} + i\Omega_1\left(\rho_{bb} - \rho_{aa}\right) \\ & + i\Omega_-\rho_{cb} - i\Omega_+\rho_{ad}, \end{aligned} \tag{2}$$

$$\begin{aligned} \dot{\rho}_{bd} = {} & i\left[(\Delta_- - \Delta_2 - \Delta_1) + i\gamma_2\right]\rho_{bd} + i\Omega_+^*\left(\rho_{dd} - \rho_{bb}\right) \\ & - i\Omega_2^*\rho_{bc} + i\Omega_1^*\rho_{ad}, \end{aligned} \tag{3}$$

$$\begin{aligned} \dot{\rho}_{ac} = {} & i\left(\Delta_- + i\gamma_3\right)\rho_{ac} + i\Omega_-\left(\rho_{cc} + \rho_{aa}\right) - i\Omega_2\rho_{ad} \\ & + i\Omega_1\rho_{bc}, \end{aligned} \tag{4}$$

$$\begin{aligned} \dot{\rho}_{bc} = {} & i\left[(\Delta_- - \Delta_1) + i\gamma_4\right]\rho_{bc} - i\Omega_-\rho_{ba} - i\Omega_2\rho_{bd} \\ & + i\Omega_+^*\rho_{dc} + i\Omega_1^*\rho_{ac}, \end{aligned} \tag{5}$$

$$\begin{aligned} \dot{\rho}_{ad} = {} & i\left[(\Delta_- - \Delta_2) + i\gamma_5\right]\rho_{ad} + i\Omega_1\rho_{bd} - i\Omega_-\rho_{cd} \\ & - i\Omega_+^*\rho_{ab} - i\Omega_2^*\rho_{ac}. \end{aligned} \tag{6}$$

The overall dephasing rates $\gamma_i (i = 1{-}5)$ are defined by $2\gamma_1 = \gamma_{bl} + \gamma_{ba}^d$, $2\gamma_2 = \gamma_{bl} + \gamma_{dl} + \gamma_{bd}^d$, $2\gamma_3 = \gamma_{cl} + \gamma_{ca}^d$, $2\gamma_4 = \gamma_{bl} + \gamma_{cl} + \gamma_{bc}^d$ and $2\gamma_5 = \gamma_{dl} + \gamma_{da} + \gamma_d \simeq \gamma_d$. Here, $\gamma_{jl} (j = b, d, c)$ is due to longitudinal optical photon emission events at low temperature, γ_{ij}^d may originate not only from electron–electron scattering and electron–phonon scattering, but also from inhomogeneous broadening due to the scattering on interface roughness, and γ_d characterizes the decay rate for the spin coherence.

Let us now define a general form of a vortex beam Ω_i characterized by a Rabi frequency

$$\Omega_i = |\Omega_i| e^{il_i\Phi}, \tag{7}$$

where l_i denotes OAM number, and Φ is the azimuthal angle. For a Laguerre–Gaussian (LG) doughnut beam, its amplitude is

$$|\Omega_i| = \varepsilon_i \left(\frac{r}{w}\right)^{|l_k|} e^{-r^2/\omega^2}, \tag{8}$$

where r represents the distance from the vortex core (cylindrical radius), w is the beam waist parameter, and ε_i is the strength of the vortex beam. In Fig. 2, we show the intensity pattern of a vortex beam for $l = 1$ (solid line), $l = 2$ (dashed line) and $l = 3$ (dotted line). One can see that the intensity of the vortex beams with different vorticities $l = 1, 2, 3$ take the same values at the position $r/w = 1$.

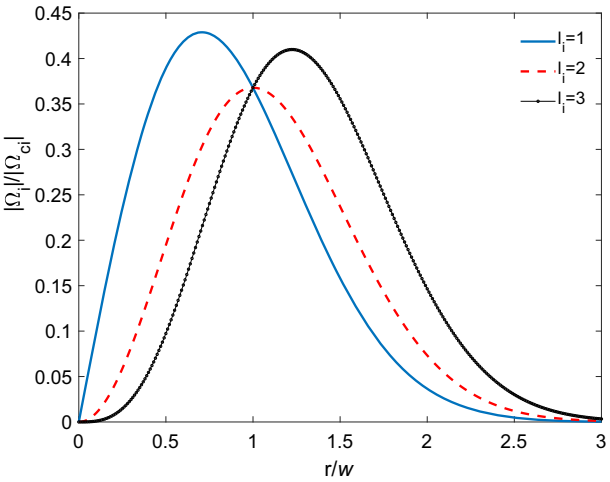

Fig. 2 Dimensionless quantity $|\Omega_i|/|\Omega_{ci}|$ given by Eq. 7 versus dimensionless distance from the vortex core r/w when $|\Omega_{ci}| = \varepsilon_i$ and for various OAM numbers

3 Model

3.1 The EIT scheme

First, we consider a scenario where the system is a mixture of two EIT subsystems in Λ configuration. The first Λ subsystem is formed by a weak probe field described by a Rabi frequency Ω_1 and a strong control field with a Rabi frequency Ω_-. Another weak probe field with a Rabi frequency Ω_+ and a strong field with a Rabi frequency Ω_2 build the second Λ subsystem.

To solve Eqs. (2)–(6), we consider a steady-state condition using a perturbation theory to denote FWM process in a closed-loop system. In the latter, the Ω_+ field is generated via the FWM pathway $|b\rangle \rightarrow |a\rangle \rightarrow |c\rangle \rightarrow |d\rangle \rightarrow |b\rangle$. We assume that both probe fields, applied Ω_1 and generated Ω_+, are much weaker than the control fields Ω_- and Ω_2. Moreover, the system is prepared initially in the ground state $|b\rangle$. Note that in each subsystem, the strong laser fields Ω_- and Ω_2 are responsible to control the propagation dynamics of the probe fields Ω_1 and Ω_+ through the quantum medium, and induce the EIT for the resonant probe beams [68]. Therefore, one can obtain the off-diagonal matrix elements of the first-order $\rho_{ab}^{(1)}$ and $\rho_{db}^{(1)}$ for the corresponding probe transitions as follows:

$$\rho_{ab}^{(1)} = \frac{-i\left(\Delta_{cb}\Delta_{ab} + |\Omega_2|^2\right)\Omega_1 + i\Omega_-\Omega_2^*\Omega_+}{\Delta_{ab}\left(\Delta_{cb}\Delta_{db} + |\Omega_2|^2\right) + \Delta_{db}|\Omega_-|^2} = a_1\Omega_1 + b_1\Omega_+, \tag{9}$$

$$\rho_{db}^{(1)} = \frac{-i\left(\Delta_{cb}\Delta_{ab} + |\Omega_-|^2\right)\Omega_+ + i\Omega_2\Omega_-^*\Omega_1}{\Delta_{db}\left(\Delta_{cb}\Delta_{ab} + |\Omega_-|^2\right) + \Delta_{ab}|\Omega_2|^2} = a_2\Omega_1 + b_2\Omega_+, \tag{10}$$

where $\Delta_{ab} = i(\Delta_1 + i\gamma_1)$, $\Delta_{cb} = i[(\Delta_- - \Delta_1) + i\gamma_4]$ and $\Delta_{db} = i[(\Delta_- - \Delta_2 - \Delta_1) + i\gamma_2]$. Here, we introduce coefficients $a_i\,(i = 1, 2)$ and $b_i\,(i = 1, 2)$ expressed as:

$$a_1 = \frac{-i\left(\Delta_{cb}\Delta_{ab} + |\Omega_2|^2\right)}{\Delta_{ab}\left(\Delta_{cb}\Delta_{db} + |\Omega_2|^2\right) + \Delta_{db}|\Omega_-|^2},$$

$$b_1 = \frac{i\Omega_-\Omega_2^*}{\Delta_{ab}\left(\Delta_{cb}\Delta_{db} + |\Omega_2|^2\right) + \Delta_{db}|\Omega_-|^2}, \tag{11}$$

$$a_2 = \frac{i\Omega_2\Omega_-^*}{\Delta_{db}\left(\Delta_{cb}\Delta_{ab} + |\Omega_-|^2\right) + \Delta_{ab}|\Omega_2|^2},$$

$$b_2 = \frac{-i\left(\Delta_{cb}\Delta_{ab} + |\Omega_-|^2\right)}{\Delta_{db}\left(\Delta_{cb}\Delta_{ab} + |\Omega_-|^2\right) + \Delta_{ab}|\Omega_2|^2}. \tag{12}$$

Under the slowly varying envelope approximation and assuming time-independent fields, the Maxwell equations for the corresponding probe fields Ω_1 and Ω_+ propagating in z direction are reduced to the coupled wave equations as follows:

$$\frac{\partial\Omega_1}{\partial z} = \frac{i\alpha_1\gamma_1}{2L}\left(a_1\Omega_1 + b_1\Omega_+\right), \tag{13}$$

$$\frac{\partial\Omega_+}{\partial z} = \frac{i\alpha_+\gamma_2}{2L}\left(a_2\Omega_1 + b_2\Omega_+\right). \tag{14}$$

Here, α_1 and α_+ are the optical depths of the corresponding probe fields, and L is the length of the medium. We assume $\Omega_1(z=0) = \Omega_1(0)$ and $\Omega_+(z=0) = 0$ at the entrance of the medium. By solving the coupled wave Eqs. (13) and (14), we obtain the expressions for the Rabi frequency of Ω_1 and Ω_+ fields:

$$\Omega_1(z) = \frac{A_1 - B_2}{A}\Omega_1(0)\left[\sinh\left(\frac{A}{4L}z\right) + \frac{A}{A_1 - B_2}\cosh\left(\frac{A}{4L}z\right)\right]e^{\frac{A_1+B_2}{4L}z}, \tag{15}$$

$$\Omega_+(z) = \frac{2A_2}{A}\Omega_1(0)\sinh\left(\frac{A}{4L}z\right)e^{\frac{A_1+B_2}{4L}z}, \tag{16}$$

where we introduced parameters

$$A_1 = i\alpha_1\gamma_1 a_1, \quad B_1 = i\alpha_1\gamma_1 b_1, \tag{17}$$

$$A_2 = i\alpha_+\gamma_2 a_2, \quad B_2 = i\alpha_+\gamma_2 b_2, \tag{18}$$

$$A = \sqrt{(A_1 - B_2)^2 + 4A_2B_1}. \tag{19}$$

Equation (16) characterizes the propagation of generated probe light through the medium. Note that the coherence term $\rho_{db}^{(1)}$ can be easily obtained by substituting Eqs. (15) and (16) into Eq. (10):

$$\rho_{db}^{(1)} = a_2\Omega_1(0)\left[\frac{A_1}{A}\sinh\left(\frac{A}{4L}z\right) + \cosh\left(\frac{A}{4L}z\right)\right]e^{\frac{A_1+B_2}{4L}z}. \tag{20}$$

3.2 The CPT scheme

In this section, we consider the atom-light coupling configuration where Ω_2 and Ω_+ fields are strong and one of the Λ subsystems is put in a CPT (dark) state

$$|D\rangle = c_b|b\rangle - c_c|c\rangle, \tag{21}$$

where

$$c_b = \frac{\Omega_2}{\sqrt{|\Omega_2|^2 + |\Omega_+|^2}}, \quad c_c = \frac{\Omega_+}{\sqrt{|\Omega_2|^2 + |\Omega_+|^2}}. \tag{22}$$

Fields with Rabi frequencies Ω_1 and Ω_- are considered to be weak probe pulses. Consequently, this weak pulse pair propagates in a coherently prepared medium interacting with

the upper legs of the double scheme. By considering the above conditions, we can obtain the coherence terms as follows:

$$\rho_{ab}^{(1)} = \frac{-i|c_b|^2\Omega_1 + ic_c c_b^*\Omega_-}{\Delta_{ab}} = c_1\Omega_1 + d_1\Omega_-, \tag{23}$$

$$\rho_{ac}^{(1)} = \frac{ic_b c_c^*\Omega_1 - i|c_c|^2\Omega_-}{\Delta_{ac}} = c_2\Omega_1 + d_2\Omega_-, \tag{24}$$

where $\Delta_{ac} = i(\Delta_- + i\gamma_3)$. The coefficients $c_i (i = 1, 2)$ and $d_i (i = 1, 2)$ read:

$$c_1 = \frac{-i|c_b|^2}{\Delta_{ab}}, \quad d_1 = \frac{ic_c c_b^*}{\Delta_{ab}}, \tag{25}$$

$$c_2 = \frac{ic_b c_c^*}{\Delta_{ac}}, \quad d_2 = \frac{-i|c_c|^2}{\Delta_{ac}}. \tag{26}$$

The following coupled wave equations for the two probe fields Ω_1 and Ω_- along the z direction can be obtained under the slowly varying envelope approximation and for time-independent fields:

$$\frac{\partial\Omega_1}{\partial z} = \frac{i\alpha_1\gamma_1}{2L}\left(c_1\Omega_1 + d_1\Omega_-\right), \tag{27}$$

$$\frac{\partial\Omega_-}{\partial z} = \frac{i\alpha_-\gamma_3}{2L}\left(c_2\Omega_1 + d_2\Omega_-\right), \tag{28}$$

where α_1 and α_- are the optical depths of the corresponding applied weak and generated probe fields. Assuming $\Omega_1(z = 0) = \Omega_1(0)$ and $\Omega_-(z = 0) = 0$, the analytical expressions for the Rabi frequency of the Ω_1 and Ω_- are obtained using the coupled Eqs. (27) and (28)

$$\Omega_1(z) = \frac{C_1 - D_2}{C}\Omega_1(0)\left[\sinh\left(\frac{C}{4L}z\right) + \frac{C}{C_1 - D_2}\cosh\left(\frac{A}{4L}z\right)\right]e^{\frac{C_1+D_2}{4L}z}, \tag{29}$$

$$\Omega_-(z) = \frac{2C_2}{C}\Omega_1(0)\sinh\left(\frac{C}{4L}z\right)e^{\frac{C_1+D_2}{4L}z}, \tag{30}$$

where

$$C_1 = i\alpha_1\gamma_1 c_1, \quad D_1 = i\alpha_1\gamma_1 d_1, \tag{31}$$

$$C_2 = i\alpha_-\gamma_3 c_2, \quad D_2 = i\alpha_-\gamma_3 d_2, \tag{32}$$

$$C = \sqrt{(C_1 - D_2)^2 + 4C_2 D_1}. \tag{33}$$

Subsequently, the steady state form of the coherence term $\rho_{ac}^{(1)}$ can be expressed as:

$$\rho_{ac}^{(1)} = c_2\Omega_1(0)\left[\frac{C_1}{C}\sinh\left(\frac{C}{4L}z\right) + \cosh\left(\frac{C}{4L}z\right)\right]e^{\frac{C_1+D_2}{4L}z}. \tag{34}$$

3.3 The ESC scheme

In this section, we consider the situation where Ω_- and Ω_1 are the weak probe light beams, and the system remains in upper level $|a\rangle$. For the Maxwell–Bloch equations, we consider a steady-state condition assuming perturbation theory to denote FWM. Here, Ω_1 can be generated via FWM pathway $|a\rangle \to |c\rangle \to |d\rangle \to |b\rangle \to |a\rangle$. In this case, both probe fields

Ω_1 and Ω_- are much weaker than the control field $\Omega_+$and Ω_2. The off-diagonal matrix elements then read

$$\rho_{ab}^{(1)} = \frac{-i\Omega_+\Omega_2^*\Omega_- + i(\Delta_{ac}\Delta_{ad} + |\Omega_2|^2)\Omega_1}{\Delta_{ab}\Delta_{ac}\Delta_{ad} + \Delta_{ac}|\Omega_+|^2 + \Delta_{ab}|\Omega_2|^2} = g_1\Omega_- + h_1\Omega_1, \tag{35}$$

$$\rho_{ac}^{(1)} = \frac{-i(\Delta_{ab}\Delta_{ad} + |\Omega_+|^2)\Omega_- - i\Omega_2\Omega_+^*\Omega_1}{\Delta_{ab}\Delta_{ac}\Delta_{ad} + \Delta_{ac}|\Omega_+|^2 + \Delta_{ab}|\Omega_2|^2} = g_2\Omega_- + h_2\Omega_1, \tag{36}$$

where $\Delta_{ab} = i(\Delta_1 + i\gamma_1)$, $\Delta_{ac} = i(\Delta_- + i\gamma_3)$ and $\Delta_{ad} = i[(\Delta_- - \Delta_2) + i\gamma_5]$. The Maxwell equations describing the propagation of two laser fields Ω_1 and Ω_- take the form

$$\frac{\partial\Omega_-}{\partial z} = \frac{i\alpha_-\gamma_3}{2L}\left(g_1\Omega_- + h_1\Omega_1\right), \tag{37}$$

$$\frac{\partial\Omega_1}{\partial z} = \frac{i\alpha_1\gamma_1}{2L}\left(g_2\Omega_- + h_2\Omega_1\right), \tag{38}$$

with

$$\begin{aligned} g_1 &= \frac{-i\left(\Delta_{ab}\Delta_{ad} + |\Omega_+|^2\right)}{\Delta_{ab}\Delta_{ac}\Delta_{ad} + \Delta_{ac}|\Omega_+|^2 + \Delta_{ab}|\Omega_2|^2}, \\ h_1 &= \frac{i\Omega_2\Omega_+^*}{\Delta_{ab}\Delta_{ac}\Delta_{ad} + \Delta_{ac}|\Omega_+|^2 + \Delta_{ab}|\Omega_2|^2}, \\ g_2 &= \frac{i\Omega_+\Omega_2^*}{\Delta_{ab}\Delta_{ac}\Delta_{ad} + \Delta_{ac}|\Omega_+|^2 + \Delta_{ab}|\Omega_2|^2}, \end{aligned} \tag{39}$$

$$h_2 = \frac{-i\left(\Delta_{ac}\Delta_{ad} + |\Omega_2|^2\right)}{\Delta_{ab}\Delta_{ac}\Delta_{ad} + \Delta_{ac}|\Omega_+|^2 + \Delta_{ab}|\Omega_2|^2}, \tag{40}$$

where α_- and α_1 show the optical depths of the corresponding applied weak and generated probe fields. We consider that $\Omega_-(z=0) = \Omega_-(0)$ and $\Omega_1(z=0) = 0$ at the entrance to the medium ($z = 0$). Solving the coupled Maxwell equations then leads to

$$\Omega_-(z) = \frac{G_1 - H_2}{G}\Omega_-(0)\left[\sinh\left(\frac{G}{4L}z\right) + \frac{G}{G_1 - H_2}\cosh\left(\frac{G}{4L}z\right)\right]e^{\frac{G_1+H_2}{4L}z}, \tag{41}$$

$$\Omega_1(z) = \frac{G_2}{G}\Omega_-(0)\left[e^{\frac{G}{4L}z} - e^{-\frac{G}{4L}z}\right]e^{\frac{G_1+H_2}{4L}z}, \tag{42}$$

where

$$G_1 = i\alpha_-\gamma_1 g_1, \quad H_1 = i\alpha_-\gamma_1 h_1, \tag{43}$$

$$G_2 = i\alpha_1\gamma_2 g_2, \quad H_2 = i\alpha_1\gamma_2 h_2, \tag{44}$$

$$G = \sqrt{(G_1 - H_2)^2 + 4G_2H_1}. \tag{45}$$

One can also find the analytical form of the coherence term $\rho_{ab}^{(1)}$ as

$$\rho_{ab}^{(1)} = g_2\Omega_-(0)\left[\frac{G_1}{G}\sinh\left(\frac{G}{4L}z\right) + \cosh\left(\frac{G}{4L}z\right)\right]e^{\frac{G_1+H_2}{4L}z}. \tag{46}$$

The imaginary and real parts of the coherence term $\rho_{ab}^{(1)}$ correspond to the absorption and dispersion of generated probe light.

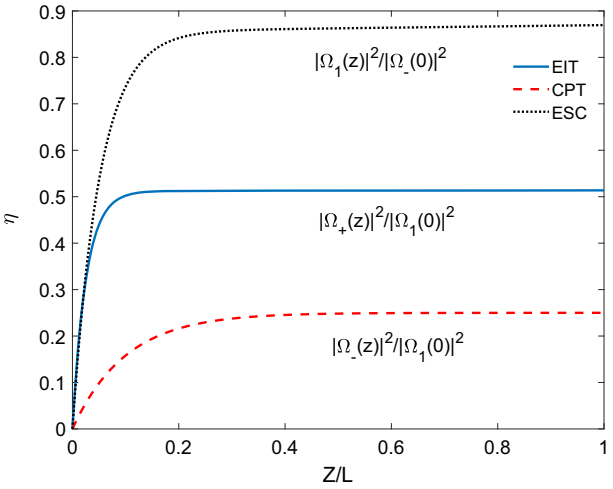

Fig. 3 Intensity of generated probe light $|\Omega_+(z)|^2/|\Omega_1(0)|^2$ (solid line) ,$|\Omega_-(z)|^2/|\Omega_1(0)|^2$ (dashed line) and $|\Omega_1(z)|^2/|\Omega_-(0)|^2$ (dotted line) versus dimensionless distance. The other selected parameters are $\gamma_1 = \gamma_2 = \gamma$, $\gamma_4 = 0.001\gamma$, $\Delta_1 = \Delta_- = \Delta_2 = 0$, $\Omega_2 = \Omega_- = \gamma$ (EIT), $\gamma_1 = \gamma_3 = \gamma$, $\Delta_1 = \Delta_- = 0$, $\Omega_2 = \Omega_+ = \gamma$, (CPT) and $\gamma_2 = \gamma_4 = \gamma$, $\gamma_5 = 0.0001\gamma$, $\Delta_1 = \Delta_- = \Delta_2 = 0$, $\Omega_+ = 1\gamma$, $\Omega_2 = 0.77\gamma$ (ESC)

4 Exchange of optical vortices

In the following, we analyze transfer of the optical vortex assisted by the FWM mechanism. Equations (16) (EIT case), (30) (CPT case) and (42) (ESC case) show that the transfer of OAM to the generated FWM is possible for all these cases. We compare in Fig. 3 the high-efficiency FWM conversion assisted by the EIT, CPT and ESC effects. The FWM efficiency, defined by the energy of the output generated probe beam and the energy of the input applied probe beam, can be expressed by $\eta = \frac{I_f}{I_i}$. Obviously, the generated probe beams for all three cases slightly oscillate at the beginning of the medium when the absorption losses occur. However, going deeper through the medium the losses disappear. We find that the efficiency of the generated light is much higher for the case with ESC. In particular, the FWM efficiency is as high as 0.8 with the assistance of ESC.

Therefore, in the following, we consider the exchange of vortices assisted by the ESC as it results in a higher FWM efficiency. Specifically, we analyze the transfer of the OAM from the coupling field Ω_2 to the generated probe field Ω_1. In this case, the coupling field Ω_2 is characterized by Rabi frequency given by Eqs. (7)–(8) where $k = 2$. The second coupling control fields is assumed to be without any vortices $\Omega_- = |\Omega_-|$. It is clear from Eq. (41) that the generated FWM beam $\Omega_1$acquires the same vorticity as of the coupling field Ω_s during its propagation as a result of the FWM process.

In Fig. 4, we display the intensity distribution, phase profile and absorption of generated probe light for different OAM numbers in the presence of spin coherence, i.e., $l_2 = 0, 1, 2, 3$. Clearly, the intensity and phase profiles illustrate a single vortex case. When $l_2 = 0$, the FWM-generated field is a Gaussian wave. A doughnut (ring) appears in the intensity distribution with a zero-intensity at its center for the nonzero l_2. The higher the OAM number is, the larger the zero-intensity hole is. When $l_2 = 3$, the FWM beam has a relatively large hole, indicating a higher OAM index. In the phase profile, no vortex is observed when $l_2 = 0$

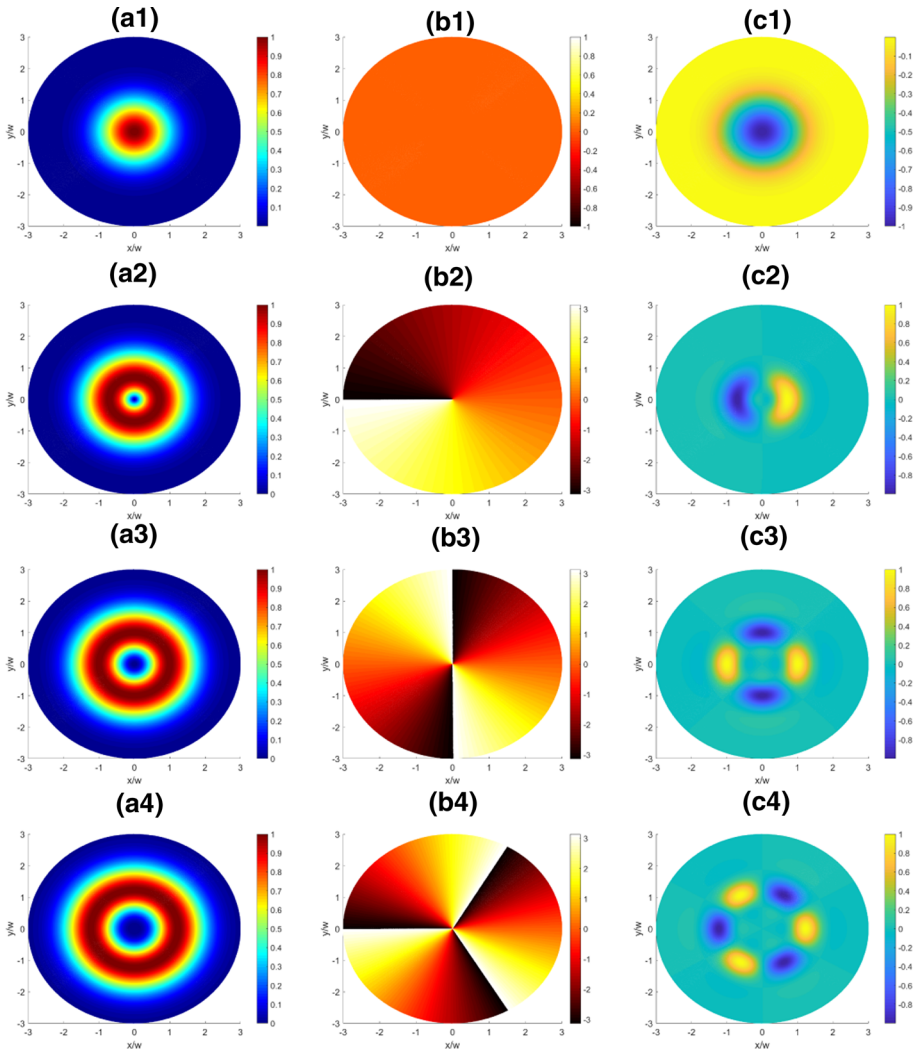

Fig. 4 Intensity (ai), phase (bi) and normalized absorption (ci) (i=1-4) of generated probe light versus normalized positions x/w and y/w when the control field Ω_2 has optical vortices with OAM of $l_2 = 0, 1, 2, 3$. Here, $\Omega_+ = \gamma$,$\varepsilon_2 = 0.77\gamma$, $\gamma_5 = 0.0001\gamma$ and $\Delta_1 = \Delta_- = \Delta_2 = 0$

showing a Gaussian-shaped wavefront of the laser field with a normal phase. The number of 2π cycles around the circumference corresponds the OAM number l_2. The absorption profile of the FWM-generated beam changes periodically when the winding number is nonzero, illustrating a number of absorption and gain maxima equal to the winding number of the weak probe field l_2. The absorption profile shows a l_2-fold symmetry distributed in regions of optical transparency.

Finally, we study the effect of the ESC decay rate when OAM number is equal to $l_2 = 1$ (Fig. 5) and $l_2 = 2$ (Fig. 6) on the absorption and dispersion of the generated probe light given by Eq. 46. The absorption and dispersion of generated probe light are plotted against the azimuthal phase. We find that the absorption and dispersion properties of the system can

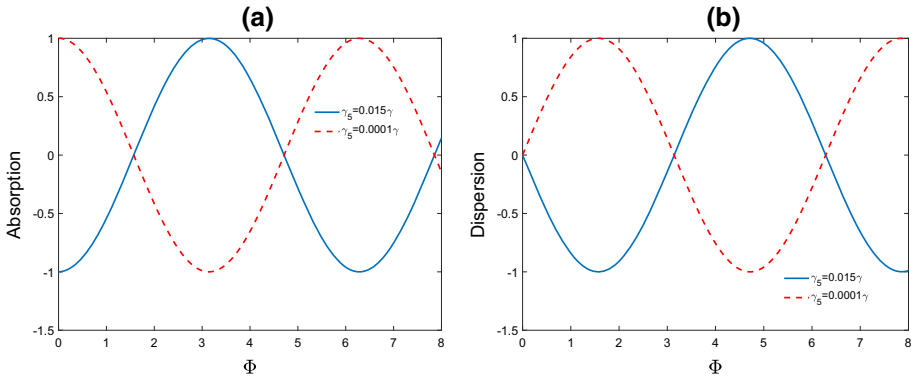

Fig. 5 Normalized absorption (**a**) and dispersion (**b**) part of generated probe light giving by Eq. 46 versus azimuthal angle of vortex field for different value of spin coherence decay rate. The selected parameters are $l_2 = 1, r/w = 1$ and others are same as Fig. 4

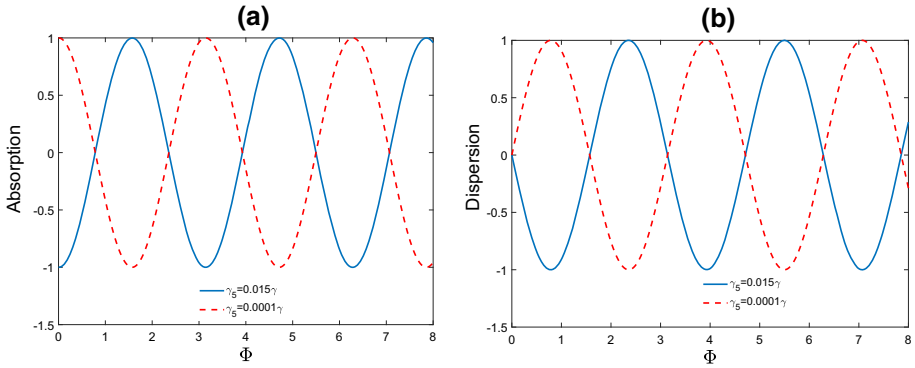

Fig. 6 Normalized absorption (**a**) and dispersion (**b**) part of generated probe light giving by Eq. 46 versus azimuthal angle of vortex field for different value of spin coherence decay rate. The selected parameters are $l_2 = 1, r/w = 1$ and others are same as Fig. 4

change in space significantly via the effect of spin coherence decay rate. This indicates that the spin coherence decay rate has a critical role on an efficient exchange of optical vortices and can result in a lossless propagation of beams carrying the OAM.

5 Conclusions

In summary, we have analyzed the effect of OAM transfer between optical fields in a quantum well waveguide structure effectively comprising two Λ type or double V-type configurations. Specifically, we considered three situations where the system is dominated by either EIT , CPT or ESC interaction regimes. In the EIT regime the system is initially prepared in a lower ground level, while in the CPT case the system is trapped in a superposition of two lower ground states. In ESC regime, however, we prepare the system in an upper excited state. We found that the efficiency of the FWM can be improved via the ESC. We let then one of the control fields to carry an OAM, while the second control field is not a vortex beam. The intensity of one of the probe fields is zero at the entrance. Subsequently, the generated probe

field can obtain the same OAM as the vortex control beam during the propagation. We have also shown that the spatially dependent absorption and dispersion of the waveguide can be strongly modified by the ESC. As a result, the spin coherence decay rate plays an important role to achieve an efficient transfer of optical vortices between different frequencies.

Acknowledgements Seyyed Hossein Asadpour and Edris Faizabadi would like to thank the Iran National Science Foundation (INSF) and Research deputy of Iran University of Science and Technology (nr. 98017089).

References

1. S.E. Harris, Phys. Today **50**, 36 (1997)
2. M. Fleischhauer, A. Imamoglu, J.P. Marangos, Rev. Mod. Phys. **77**, 633–673 (2005)
3. P. Kral, I. Thanopulos, M. Shapiro, Rev. Mod. Phys. **79**, 53–77 (2007)
4. N.V. Vitanov, A.A. Rangelov, B.W. Shore, K. Bergmann, Rev. Mod. Phys. **89**, 015006 (2017)
5. M.O. Scully, Phys. Rev. Lett. **67**, 1855–1858 (1991)
6. J.B. Pendry, Phys. Rev. Lett. **85**, 3966–3969 (2000)
7. L. Hau, S. Harris, Z. Dutton, C. Behroozi, Nature **397**, 594–598 (1999)
8. M .M. Kash, V .A. Sautenkov, A .S. Zibrov, L. Hollberg, Ge R Welch, M .D. Lukin, Y. Rostovtsev, E .S. Fry, M .O. Scully, Phys. Rev. Lett. **82**, 5229–5232 (1999)
9. L.J. Wang, A. Kuzmich, A. Dogariu, Nature **406**, 277–279 (2000)
10. C. Liu, Z. Dutton, C. Behroozi, L.V. Hau, Nature **409**, 490–493 (2001)
11. D.F. Phillips, A. Fleischhauer, A. Mair, R.L. Walsworth, M.D. Lukin, Phys. Rev. Lett. **86**, 783–786 (2001)
12. M .O. Scully, Phys. Rep. **219**, 191–201 (1992)
13. H. Schmidt, A. Imamoglu, Opt. Lett. **21**, 1936–1938 (1996)
14. H.R. Hamedi, A. Khaledi-Nasab, A. Raheli, Opt. Spectrosc. **115**, 544–551 (2013)
15. Y.-P. Niu, S.-Q. Gong, Phys. Rev. A **73**, 053811 (2006)
16. H.R. Hamedi, G. Juzeliūnas, Phys. Rev. A **91**, 053823 (2015)
17. M. Fleischhauer, M.D. Lukin, Phys. Rev. Lett. **84**, 5094–5097 (2000)
18. G. Juzeliūnas, H.J. Carmichael, Phys. Rev. A **65**, 021601 (2002)
19. A.S. Zibrov, A.B. Matsko, O. Kocharovskaya, Y.V. Rostovtsev, G.R. Welch, M.O. Scully, Phys. Rev. Lett. **88**, 103601 (2002)
20. M.D. Eisaman, A. André, F. Massou, M. Fleischhauer, A.S. Zibrov, M.D. Lukin, Nature **438**, 837 (2005)
21. M. Fleischhauer, S.-Q. Gong, Phys. Rev. Lett. **88**, 070404 (2002)
22. G. Juzeliūnas, M. Mašalas, M. Fleischhauer, Phys. Rev. A **67**, 023809 (2003)
23. D.A. Braje, V. Balić, G.Y. Yin, S.E. Harris, Phys. Rev. A **68**, 041801 (2003)
24. F.-X. Esnault, E. Blanshan, E.N. Ivanov, R.E. Scholten, J. Kitching, E.A. Donley, Phys. Rev. A **88**, 042120 (2013)
25. S.A. Hawkins, E.J. Gansen, M.J. Stevens, A.L. Smirl, I. Rumyantsev, R. Takayama, N.H. Kwong, R. Binder, D.G. Steel, Phys. Rev. B **68**, 035313 (2003)
26. S. Marcinkevicius, A. Gushterov, J.P. Reithmaier, Appl. Phys. Lett. **92**, 041113 (2008)
27. T. Li, H. Wang, N.H. Kwong, R. Binder, Opt. Express **11**, 3298–3303 (2003)
28. A. Imamoglu, Opt. Commun. **179** (2000)
29. W.W. Chow, H.C. Schneider, M.C. Phillips, Phys. Rev. A **68**, 053802 (2003)
30. M.C. Phillips, H. Wang, I. Rumyantsev, N.H. Kwong, R. Takayama, R. Binder, Phys. Rev. Lett. **91**, 183602 (2003)
31. M. Yan, E.G. Rickey, Y.-F. Zhu, J. Opt. Soc. Am. B **18**, 1057–1062 (2001)
32. D.J. Fulton, S. Shepherd, R.R. Moseley, B.D. Sinclair, M.H. Dunn, Phys. Rev. A **52**, 2302–2311 (1995)
33. J. Gea-Banacloche, Y.Q. Li, S.Z. Jin, M. Xiao, Phys. Rev. A **51**, 576–584 (1995)
34. L. Allen, M.J. Padgett, M. Babiker, Progress Opt. **39**, 291–372 (1999)
35. M. Padgett, J. Courtial, L. Allen, Phys. Today **57**, 35 (2004)
36. A. Mair, A. Vaziri, G. Weihs, A. Zeilinger, Nature **412**, 313–316 (2011)
37. J. Leach, B. Jack, J. Romero, A.K. Jha, A.M. Yao, S. Franke-Arnold, D.G. Ireland, R.W. Boyd, S.M. Barnett, M.J. Padgett, Science **329**, 662–665 (2010)
38. S. Liu, Y. Lou, J. Jing, Nat. Commun. **11**, 3875 (2020)
39. Z.-K. Su, F.-Q. Wang, R.-B. Jin, R.-S. Liang, S.-H. Liu, Opt. Commun. **281**, 5063–5066 (2008)
40. S.H. Kazemi, M. Mahmoudi, Laser Phys. Lett. **16**, 076001 (2019)
41. Z. Dutton, J. Ruostekoski, Phys. Rev. Lett. **93**, 193602 (2004)

42. R. Pugatch, M. Shuker, O. Firstenberg, A. Ron, N. Davidson, Phys. Rev. Lett. **98**, 203601 (2007)
43. T. Wang, L. Zhao, L. Jiang, S.F. Yelin, Phys. Rev. A **77**, 043815 (2008)
44. D. Moretti, D. Felinto, J.W.R. Tabosa, Phys. Rev. A **79**, 023825 (2009)
45. J. Ruseckas, A. Mekys, G. Juzeliūnas, J. Opt. **13**, 064013 (2011)
46. J. Ruseckas, A. Mekys, G. Juzeliūnas, Phys. Rev. A **83**, 023812 (2011)
47. F.A. Hashmi, M.A. Bouchene, Phys. Rev. Lett. **101**, 213601 (2008)
48. H.R. Hamedi, J. Ruseckas, G. Juzeliūnas, Phys. Rev. A **98**, 013840 (2018)
49. H.R. Hamedi, J. Ruseckas, E. Paspalakis, G. Juzeliūnas, Phys. Rev. A **99**, 033812 (2019)
50. H .R. Hamedi, E. Paspalakis, G. žlabys, G. Juzeliūnas, J. Ruseckas, Phys. Rev. A **100**, 023811 (2019)
51. X.X. Yang, Z.W. Li, Y. Wu, Phys. Lett. A **340**, 320–325 (2005)
52. J.-B. Liu, N. Liu, C.-J. Shan, T.-K. Liu, Y.-X. Huang, Phys. Rev. E **81**, 036607 (2010)
53. G.B. Serapiglia, E. Paspalakis, C. Sirtori, K.L. Vodopyanov, C.C. Phillips, Phys. Rev. Lett. **84**, 1019–1022 (2000)
54. S.M. Sadeghi, S.R. Leffler, J. Meyer, Phys. Rev. B **59**, 15388 (1999)
55. S.M. Sadeghi, H.M. van Driel, J.M. Fraser, Phys. Rev. B **62**, 15386 (2000)
56. J.F. Dynes, E. Paspalakis, Phys. Rev. B **73**, 233305 (2006)
57. M.D. Frogley, J.F. Dynes, M. Beck, J. Faist, C.C. Phillips, Nat. Mater. **5**, 175–178 (2006)
58. W.-X. Yang, X.X. Yang, R.-K. Lee, Opt. Express **17**, 15402–15408 (2009)
59. M.A. Anton, F. Carreno Oscar, G. Calderon, Sonia Melle, Opt. Commun **281**, 644–654 (2008)
60. J.-H. Li, Phys. Rev. B **75**, 155329 (2007)
61. H. Sun, S.-Q. Gong, Y.-P. Niu, S.-Q. Jin, R.-X. Li, Z.-Z. Xu, Phys. Rev. B **74**, 155314 (2006)
62. S. Evangelou, E. Paspalakis, Photon Nanostr. Fund. Appl. **9**, 168–173 (2011)
63. S.G. Kosionis, A.F. Terzis, E. Paspalakis, J. Appl. Phys. **109**, 084312 (2011)
64. S.-W. Chang, S.L. Chuang, C.J. Chang-Hasnain, H. Wang, J. Opt. Soc. Am. B **24**, 849–859 (2007)
65. Y.-F. Zhang, Z.-P. Wang, J. Qiu, Y. Hong, BYu. Appl, Phys. Lett. **115**, 171905 (2019)
66. Z.-P. Wang, Y.-F. Zhang, E. Paspalakis, BYu. Phys, Rev. A **102**, 063509 (2020)
67. J. Qiu, Z.-P. Wang, D.-S. Ding, W.-B. Li, BYu. Opt, Express **28**, 2975–2986 (2020)
68. S.A. Moiseev, B.S. Ham, Phys. Rev. A **73**, 033812 (2006)